

## Supporting Information

### Understanding the Impact of Catholyte Flow Compartment Design on the Efficiency of CO<sub>2</sub> Electrolyzers

*Michael Filippi,<sup>#1</sup> Tim Möller,<sup>#1</sup> Liang Liang,<sup>1</sup> and Peter Strasser<sup>1\*</sup>*

<sup>1</sup>The Electrochemical Energy, Catalysis, and Materials Science Laboratory, Department of Chemistry, Chemical Engineering Division, Technical University Berlin, Berlin, Germany

<sup>‡</sup>These authors contributed equally to this work

\*Corresponding author:

Peter Strasser, [pstrasser@tu-berlin.de](mailto:pstrasser@tu-berlin.de)

## Experimental

### 1.1 Electrochemical cell and electrode preparation

This study uses a PTFE-based GDE with a CuO catalyst from Johnson Matthey as cathode and a bare Ni foam (Fraunhofer IFAM, thickness of 0.45 mm) as anode in electrocatalytic testing. For cathode preparation, we use a sintered PTFE membrane (Elringklinger, 0.5 mm thickness) as substrate material and a spray coating approach to deposit the cathode catalyst layer. The catalyst powder was ultrasonically dispersed in a water/isopropanol (80:20) mixture in the presence of Nafion ionomer (Sigma-Aldrich, 5 wt. % solution). A typical ink composition used during spray coating is given in the following:

- 10 ml of water/isopropanol (80:20)
- 250 mg of CuO powder
- 13.15 mg of Nafion

Throughout the whole study, a Nafion binder amount of 5 wt. % and a CuO loading of 1 mg cm<sup>-2</sup> were used. The coated GDE was placed inside the endplate cavity and fixed to the endplate with conductive copper tape to assemble the cell. We note here that we initially place a 10 cm<sup>2</sup> sized electrode into the endplate cavity and use the electrode's edges to establish an electronic connection between the endplate/current collector and the catalyst layer, leaving an exposed active electrode area of 5 cm<sup>2</sup>. Ice cube gaskets with a 5 cm<sup>2</sup> cut-out window were used on the cathode side (35 FC-PO 100, 0.35 mm, Quintech) and on the anode side (60 FC-FKM 200, 0.5 mm, Quintech) to enable a leak-free cell setup. 3D printing (PEEK laser sintering) was utilized for manufacturing the PEEK flow compartments. The assembly of the cell is shown in more detail in Fig. S4. The anolyte and catholyte consisted of 1.0 M KHCO<sub>3</sub> with 500 ml in each electrolyte vessel. The cathode and anode compartments were separated by an anion exchange membrane (Selemion, AMV).

### 1.2 Electrochemical setup

The electrochemical testing setup is shown in Fig. S1. Besides CO<sub>2</sub> and N<sub>2</sub> mass flow controllers (Bronkhorst), back pressure regulators (Bronkhorst) were used to accurately adjust the pressure levels at the gas and liquid side of the cathode GDE. The CO<sub>2</sub> flow rate was set to 50 ml min<sup>-1</sup> for all experiments, and a second CO<sub>2</sub> flow of 150 ml min<sup>-1</sup> was used to purge the catholyte headspace and to pressurize the electrolyte. The CO<sub>2</sub> purge flow was necessary to detect the gas phase products crossing over into the catholyte. The anolyte and catholyte were circulated with individual membrane pumps (KNF, SIMDOS 10) at a constant 50 ml min<sup>-1</sup> flow rate.

Furthermore, pressure dampeners were included to reduce flow oscillations of the membrane pumps. The cell was operated with overpressure on the gas side (1.3 bar absolute pressure) and on the liquid side (1.4 bar absolute pressure) leaving a differential pressure across the GDE of 100 mbar.

### 1.3 Electrochemical measurement protocol

Electrochemical characterization was performed with a standardized protocol, including first galvanostatic measurement steps, second cyclovoltammetry (CV) and finally galvanostatic electrochemical impedance spectroscopy (GEIS).

**Galvanostatic measurement steps:** Before starting the actual reaction and application of current, the system is equilibrated at open circuit potential (OCP) for 20 min. The following current density steps were held for 20 min each before changing to the next one. Measurements were conducted for the following current density steps: 50, 100, 200, 300, 400, 500, 600 and 700 mA cm<sup>-2</sup>.

**Cyclovoltammetry (CV).** The CVs were performed in a potential window of 100 mV (-0.600 to -0.700 V<sub>Ag/AgCl</sub>). Within this potential window, 5 CVs with a constant scan rate were performed before

increasing and measuring 5 CVs again at a higher scan rate. The following scan rates were measured sequentially:

1, 2, 5, 10, 20, 50, 100, 200, 500, 700, 1000, 1500 and 2000 mV s<sup>-1</sup>.

**Galvanostatic electrochemical impedance spectroscopy (GEIS).** As a final step, GEIS was performed at current density steps of 5, 10, 20, 50, 100, 200, 300, 400, 500, 600, and 700 mA cm<sup>-2</sup>. The frequency for each step was varied between 500 kHz and 100 mHz, and the amplitude of the interference signal was set to 10% of the respective current density value set during the step.

#### 1.4 Product quantification

**Quantification of gaseous products.** The product gas leaving the cell is combined with a second CO<sub>2</sub> flow (150 ml min<sup>-1</sup>), purging the catholyte headspace and a third gas flow of nitrogen (16 ml min<sup>-1</sup>) as an internal standard for accurate flow determination. This three-component gas mixture flows into the gas chromatograph (Shimadzu, GC 2014 series). The gas chromatograph (GC) was equipped with a thermal conductivity detector (TCD) and a flame ionization detector (FID). H<sub>2</sub> and N<sub>2</sub> were detected with the TCD, whereas methane, ethylene, and CO were detected with the FID. For accurate flow determination, the nitrogen concentration from the TCD was evaluated. For the detection of CO by FID, a methanizer has been used for the conversion of CO to methane and subsequent detection.

**Quantification of liquid products.** For selected experiments, liquid samples were collected during the measurement. Those samples were taken directly at the end of each galvanostatic current step and analyzed for the amount of alcohols by liquid injection gas chromatography (Shimadzu, GC 2010 series) equipped with an FID. On top of that, carbonic acids and their salts were analyzed by high-pressure liquid chromatography (Agilent, 1200 series).

#### 1.5 Manufacturing and simulation of fluid compartments

The fluid compartments were designed with Solidworks CAD program (Solidworks 2021). After finalizing the CAD drawings of the fluid compartments, the designs were 3D printed from PEEK based on a powder sintering approach conducted by Protiq GmbH. The CFD simulations were performed with the integrated Solidworks CFD simulation tool. The parameters that were used in this study are presented in Table S1.

**Table S1:** Parameters used to set up the CFD simulations with Solidworks Flow Simulation. If not explicitly mentioned, parameters were set as default.

<b>Solidworks Flow Simulation Parameter</b>	<b>Setting</b>
<b>Analysis type</b>	Internal analysis
<b>Additional studied physical feature</b>	Gravity
<b>Fluid type</b>	Water
<b>Simulated fluid flow type</b>	Laminar and turbulent
<b>Wall condition</b>	Adiabatic
<b>Temperature</b>	293.2 K
<b>Pressure</b>	101325 Pa
<b>Mesh settings</b>	Automatic, 6
<b>Boundary condition inlet</b>	Volumetric flow set usually to $8.33 \times 10^{-7} \text{ m}^3 \text{ s}^{-1}$ (50 ml min <sup>-1</sup> )
<b>Boundary condition outlet</b>	Ambient pressure
<b>Surface boundary condition (for particle study)</b>	Real wall: 293.2 K, 1 micrometer roughness
<b>Global convergence goal</b>	Volumetric flow
<b>Surface convergence goal 1</b>	Volumetric flow at inlet surface
<b>Surface convergence goal 2</b>	Volumetric flow at outlet surface
<b>Equation based goal</b>	Goal was set to account for mass continuity
<b>Parameters for particle study</b>	100 Points, 100 $\mu\text{m}$ particle size, Nitrogen particles, 1 ml min <sup>-1</sup> nitrogen flow from the electrode surface, Accretion and gravity were set up, Wall condition: absorption

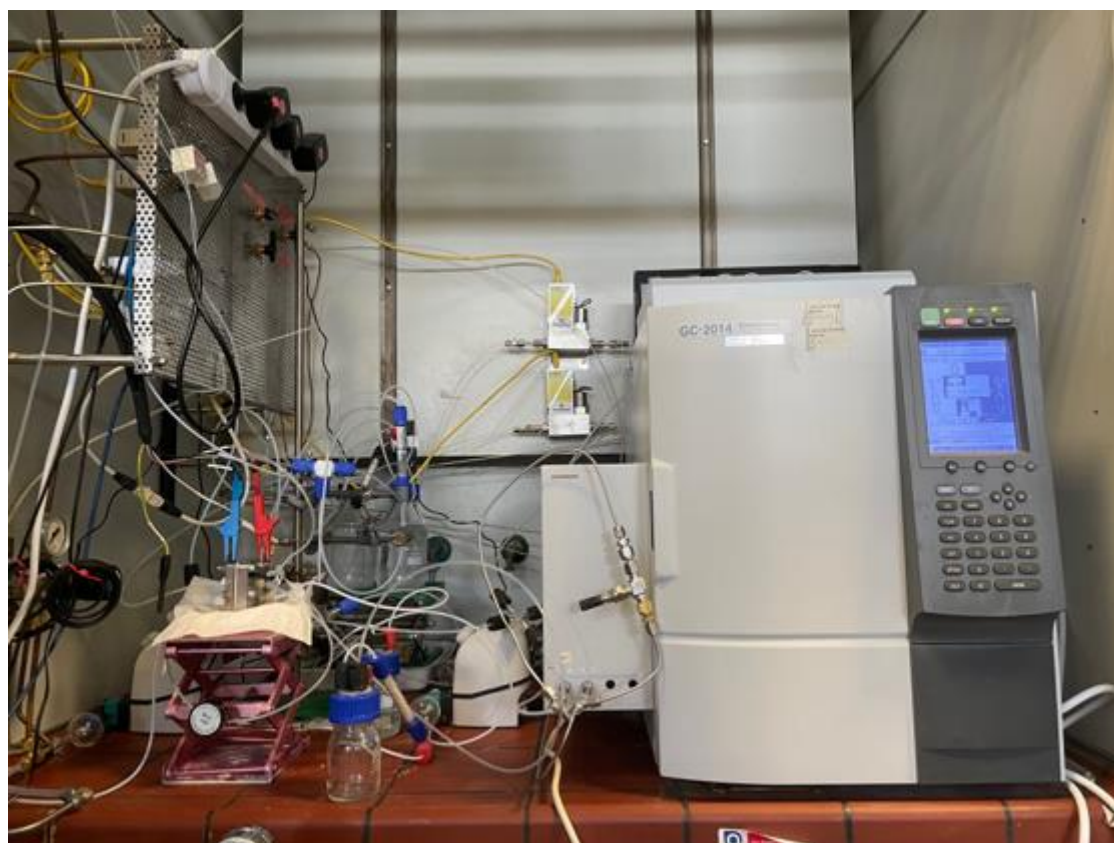
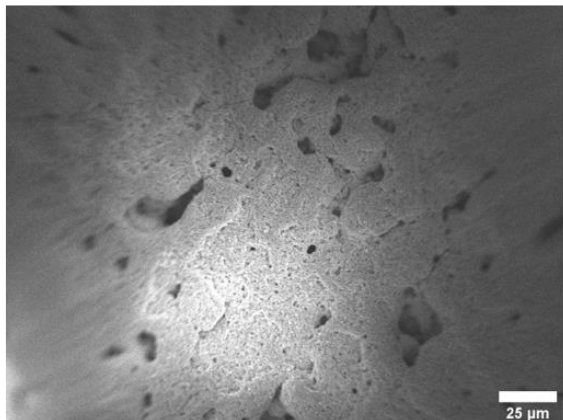
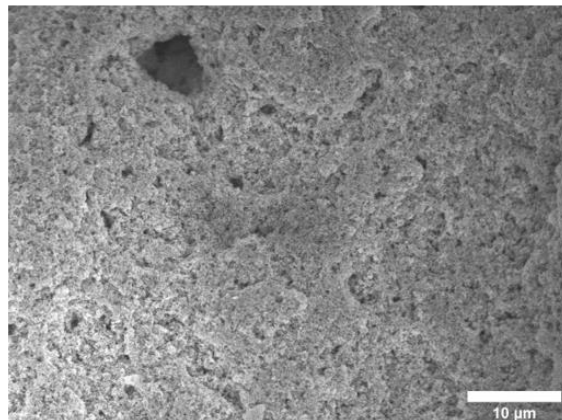


**Fig. S1.** Image of the CO<sub>2</sub>RR setup deployed for catalytic testing. The CO<sub>2</sub>RR setup includes many necessary components like GC, electrochemical flow cell, mass flow controllers, back pressure regulators and many others.

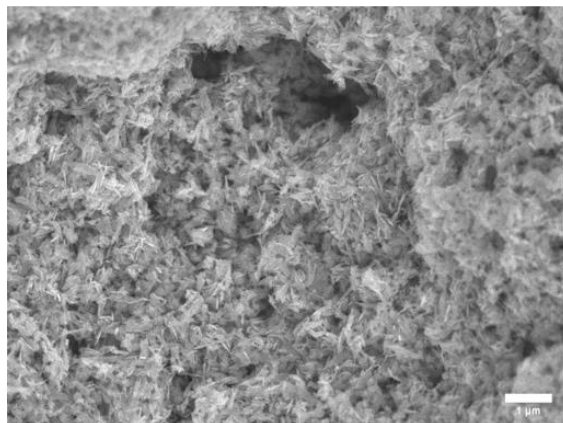
(a)



(b)



(c)



(d)

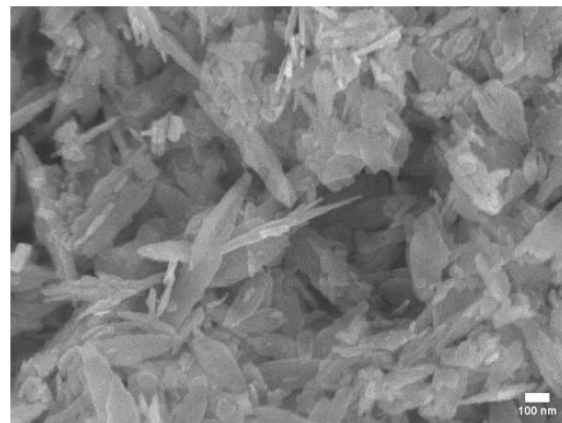
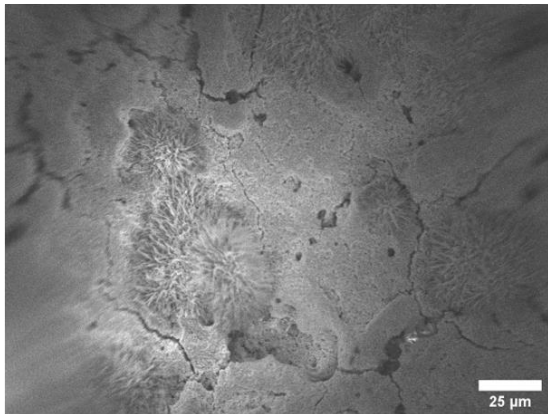
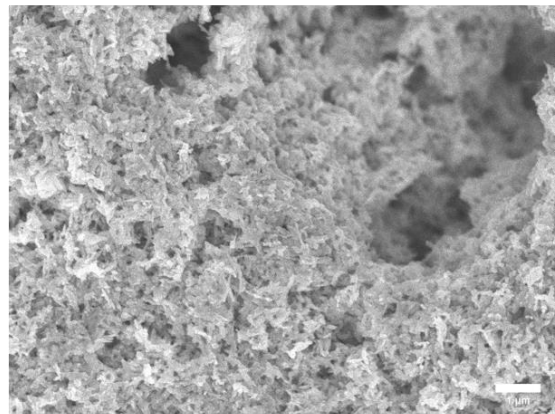


**Fig. S2.** SEM top view images of the as-prepared cathodes before electrochemical testing at various magnifications. (a) 500k magnification SEM image. (b) 2k magnification SEM image. (c) 10k magnification SEM image. (d) 50k magnification SEM image.

(a)



(b)



(c)

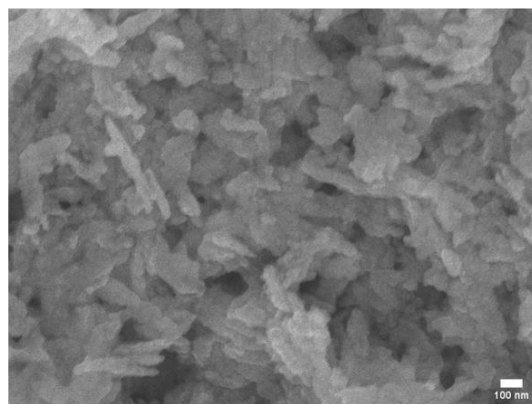


**Fig. S3.** SEM top view images of the studied Cu-GDE after electrochemical testing with the Shifted flow compartment. (a) 500k magnification SEM image. (b) 10k magnification SEM image. (c) 50k magnification SEM image. Particles tend to lose their sharp features after electrochemical testing.

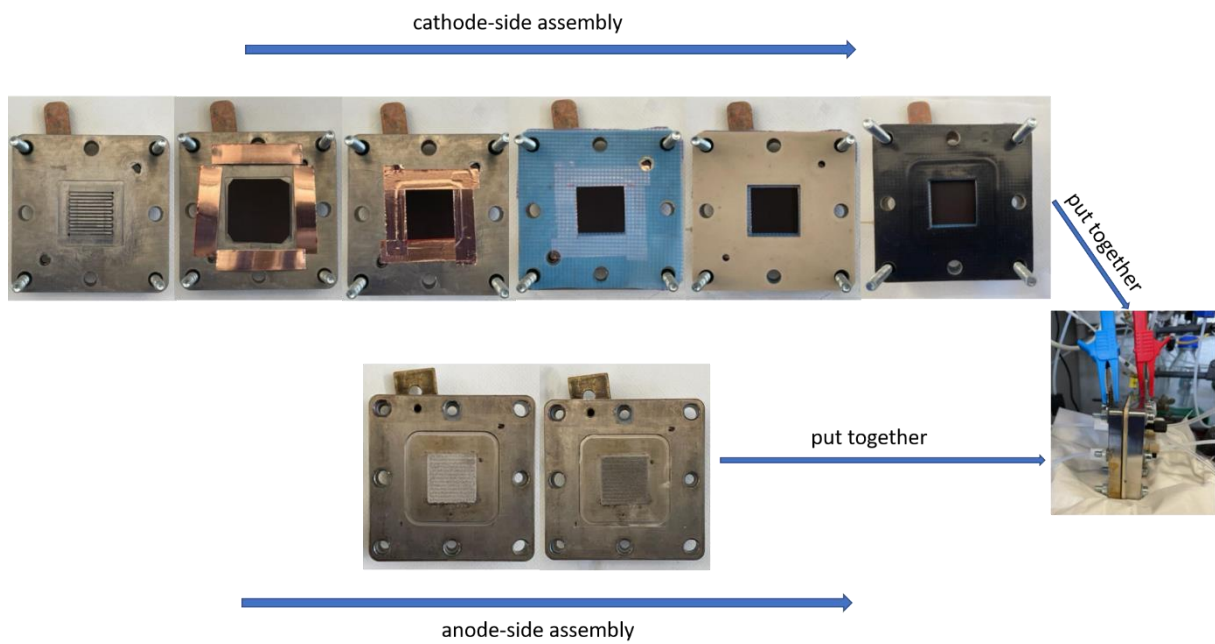


**Fig. S4.** Process steps for cell assembly. The cell was built by starting from the cathode endplate and following the steps given in this figure. The custom-made endplate on the cathode side has a 0.45 mm deep cavity with a size of 10 cm<sup>2</sup> to guarantee a plane surface when the cathode is mounted on the endplate. This is necessary to enable a leak-free operation of the cell.

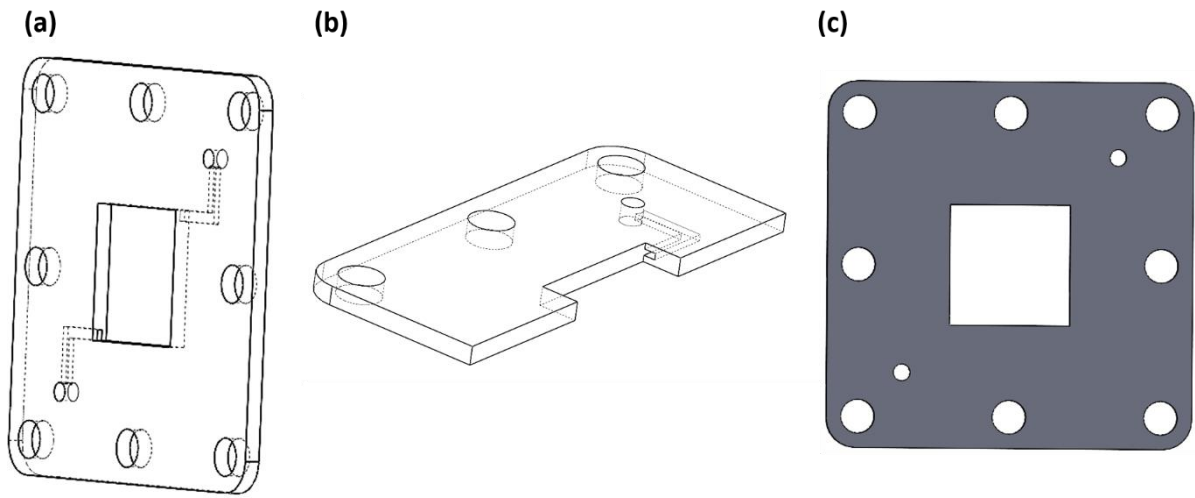
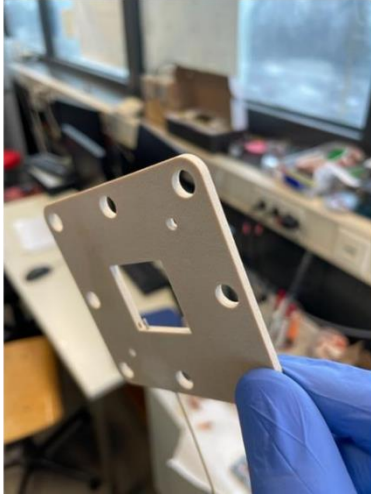
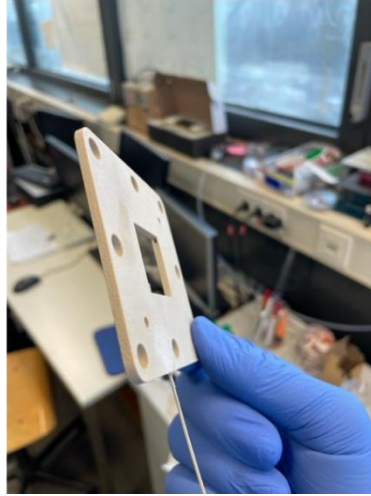


**Fig. S5.** CAD model for the Shifted flow compartment. The CAD drawings (a), (b) and (c) all show the Shifted flow compartment from different angles.

**(a)**



**(b)**



**(c)**

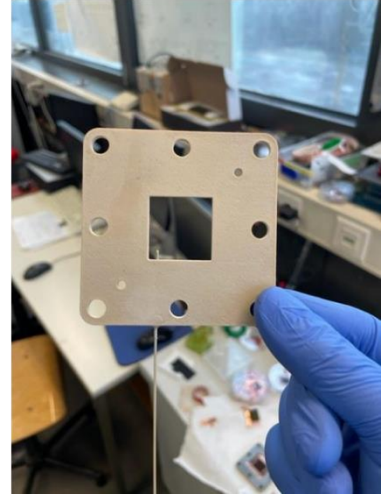


**Fig. S6.** The manufactured 3D printed PEEK Shifted flow compartment is shown from three different angles (a), (b) and (c).

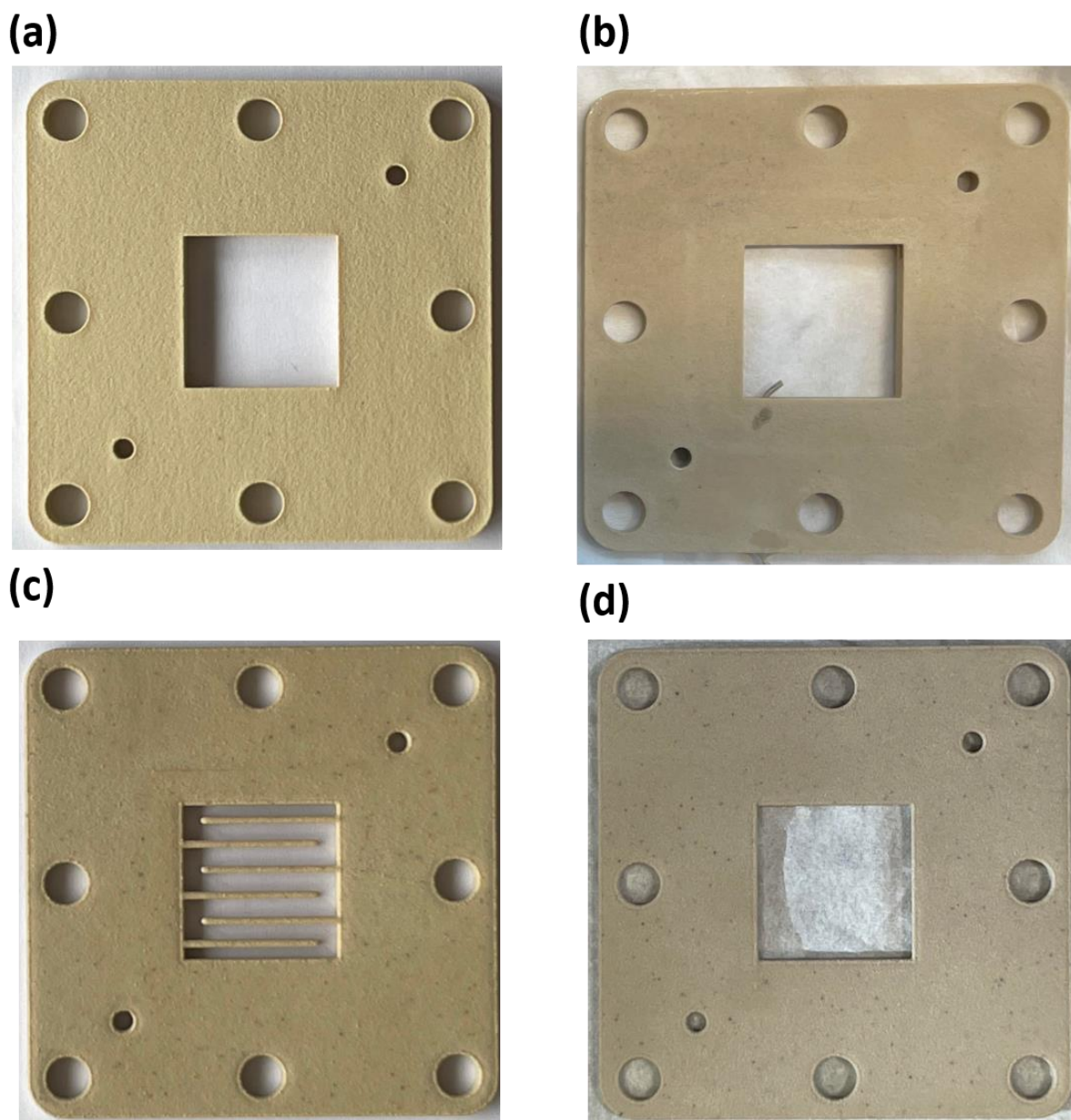


**Fig. S7.** Images of the 3D printed catholyte flow compartments used in the present study: (a) Linear wide, (b) Shifted, (c) Serpentine and (d) Linear. One can still see the employed Ag/AgCl reference electrode in (b). For mounting the reference electrode, holes were drilled into the side of the flow compartments, which enabled the placement of the reference electrode near the catalyst layer.

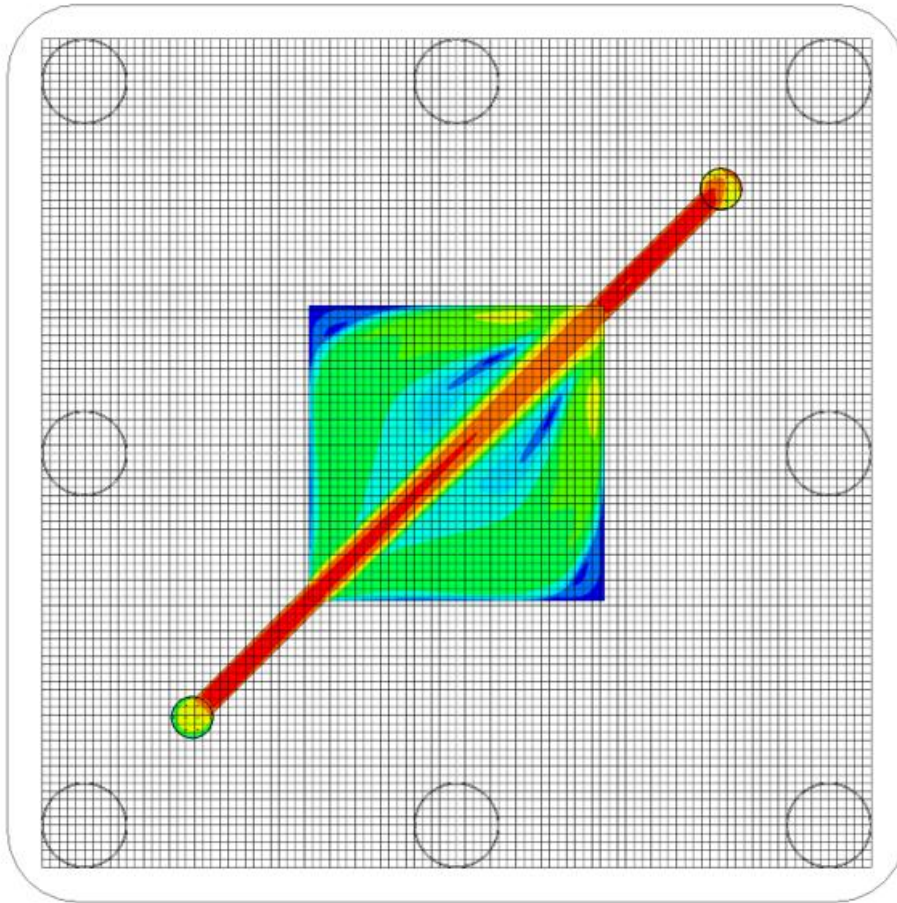


**Fig. S8.** Exemplary mesh structure used for the CFD simulations. In Solidworks CFD simulation, a mesh structure with the value of 6 for the resolution was used and created automatically.

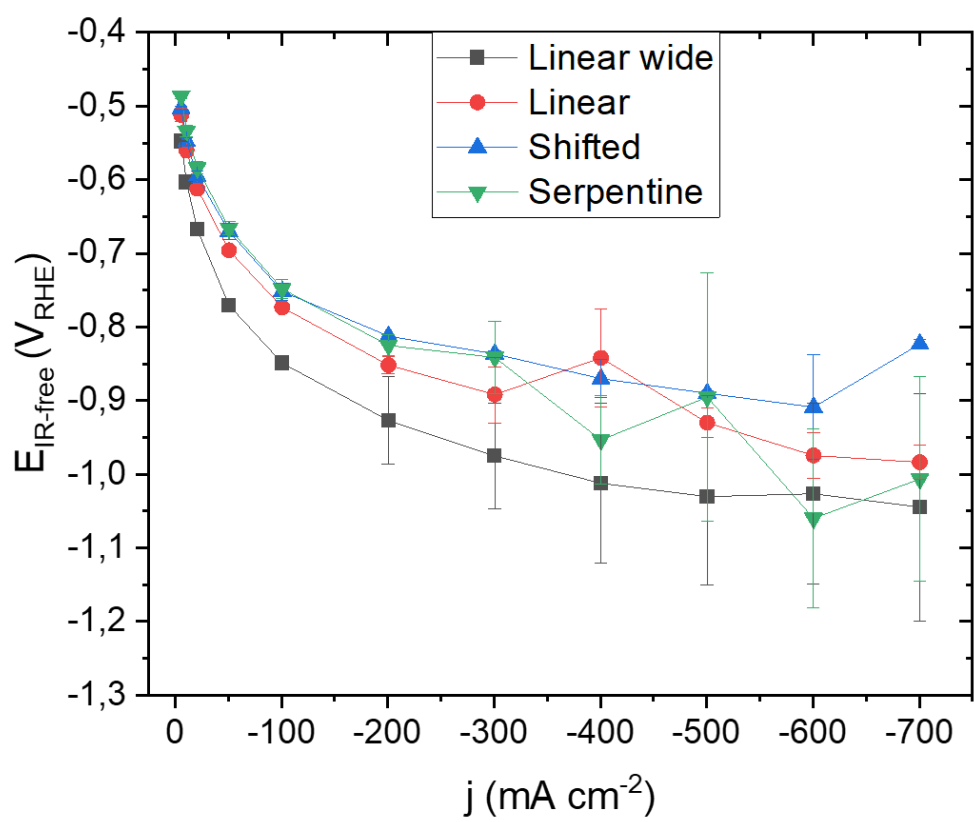


**Fig. S9.** Polarization curves of the measured flow compartments. IR-corrected cathodic potential (RHE scale) is plotted against the applied current density.

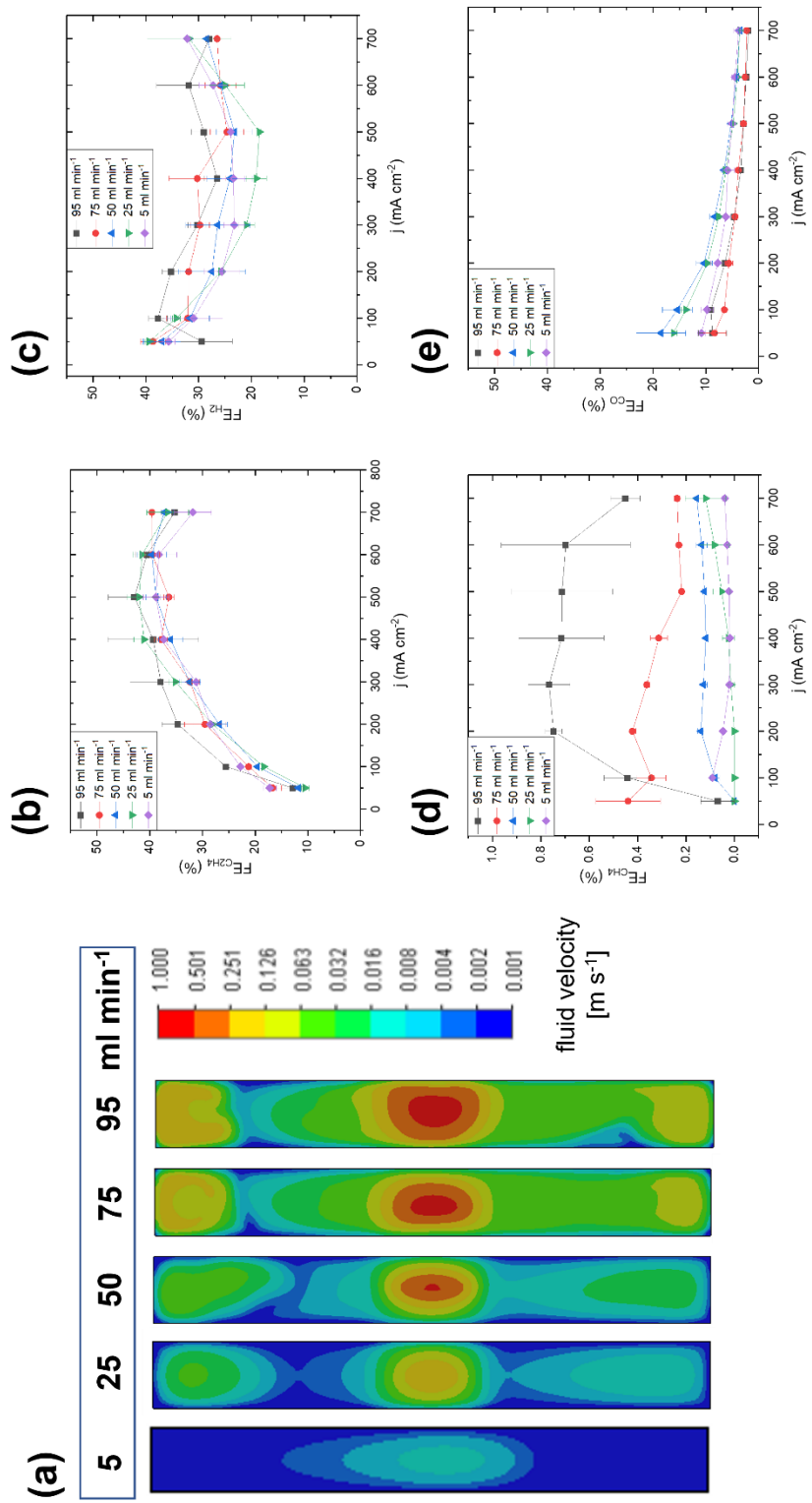


**Fig. S10.** Combined experimental and CFD study for the Linear flow compartment. (a) Cross sectional view of the center of the Linear flow compartment. Contour plots calculated for flow rates of 5, 25, 50, 75, 95  $\text{ml min}^{-1}$  are shown. Faradaic efficiency (y-axis) as a function of applied geometric current density (x-axis) for various investigated electrolyte flow rates was plotted for (b) ethylene, (c) hydrogen, (d) methane and (e) CO.

## Supplementary discussion I

In this section, we elaborate on the recommended fluid velocity range of  $0.1 - 0.01 \text{ m s}^{-1}$ . The fluid velocity range was estimated based on the CFD simulations and comparisons of the four different fluid compartments. To visualize why we proposed this range as an "optimal" fluid velocity, we added Figure S11, which provides additional information on the differences between the investigated flow compartment designs. To support this discussion, we calculated the fluid velocities along a central line, shown in Figure S11a, to directly compare the differences introduced by flow compartment design. The "Serpentine" design was not considered here due to the previously discussed specific issue of gas bubble accumulation below the ribs. Figure S11b plots the fluid velocity as a function of position across the central line, and Figure S11c provides a smaller scale for a clearer interpretation of the results.

Firstly, both Linear and Linear wide compartments show a more inhomogeneous fluid velocity distribution than the Shifted compartment, displaying a very high fluid velocity regime in the center of the flow compartment. Secondly, the two linear compartments show a lower fluid velocity at the edges of the flow compartment. In contrast, the Shifted compartment shows a much more homogenous fluid velocity along the central line of the compartment. Figure S11c shows that the Shifted compartment fluid velocity mainly reads values between  $0.01$  to  $0.1 \text{ m s}^{-1}$ . Based on the superior performance of the Shifted compartment relative to the other investigated designs, we assumed these values as being optimal for our investigated system.

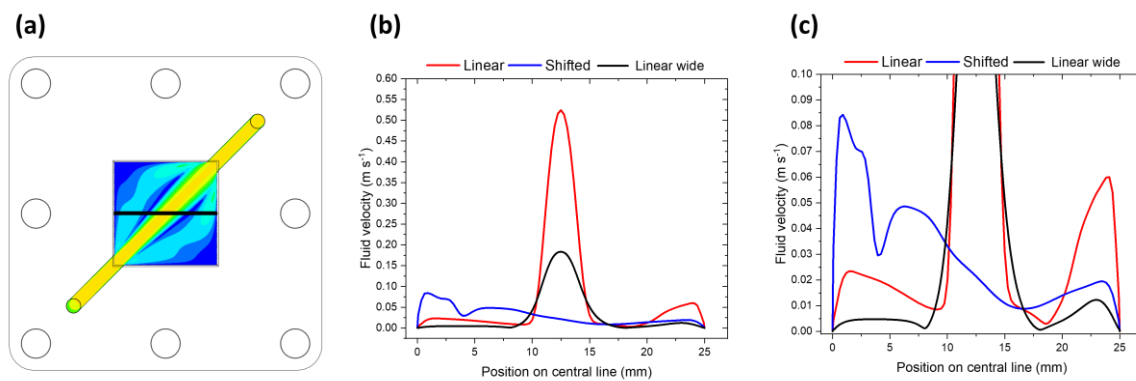


**Fig. S11.** Fluid velocity distribution analysis along a central line of the flow compartments. (a) Linear wide flow compartment is shown here, with a black line in the center of the flow compartment along which the fluid velocities were extracted. (b) Fluid velocity on the y-axis is plotted against the position on the central line on the x-axis. (c) Fluid velocity on the y-axis is plotted between  $0 - 0.1 \text{ m s}^{-1}$  against the position on the central line on the x-axis.

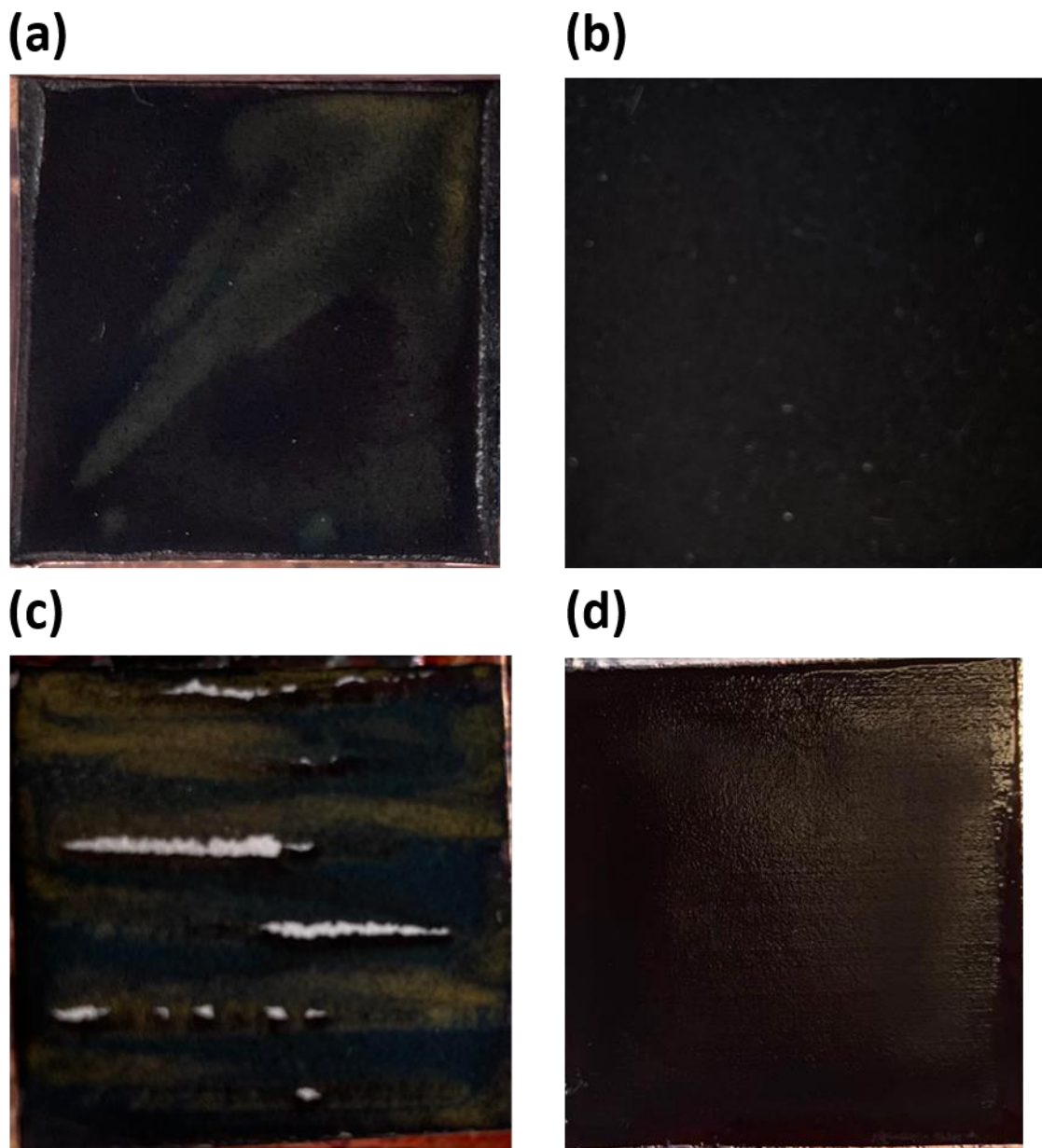


**Fig. S12.** Images of electrodes after electrochemical experiments. (a) An electrode image was taken after electrochemical testing with the Linear wide compartment. Yellow discolorations are visible. We hypothesize that this is an indication of non-optimal bubble transport. (b) An electrode image was taken after electrochemical testing with the Shifted compartment. No discolorations are visible, which suggests an optimal gas bubble transport. (c) An electrode image was taken after electrochemical testing with the Serpentine compartment. Yellow discolorations are visible, which align with the location below the PEEK ribs of the serpentine flow field. The particle study also indicates non-optimal gas bubble transport below the ribs of the flow field. (d) An electrode image was taken after testing with the Linear compartment. No discolorations are visible, which indicates optimal gas bubble transport.

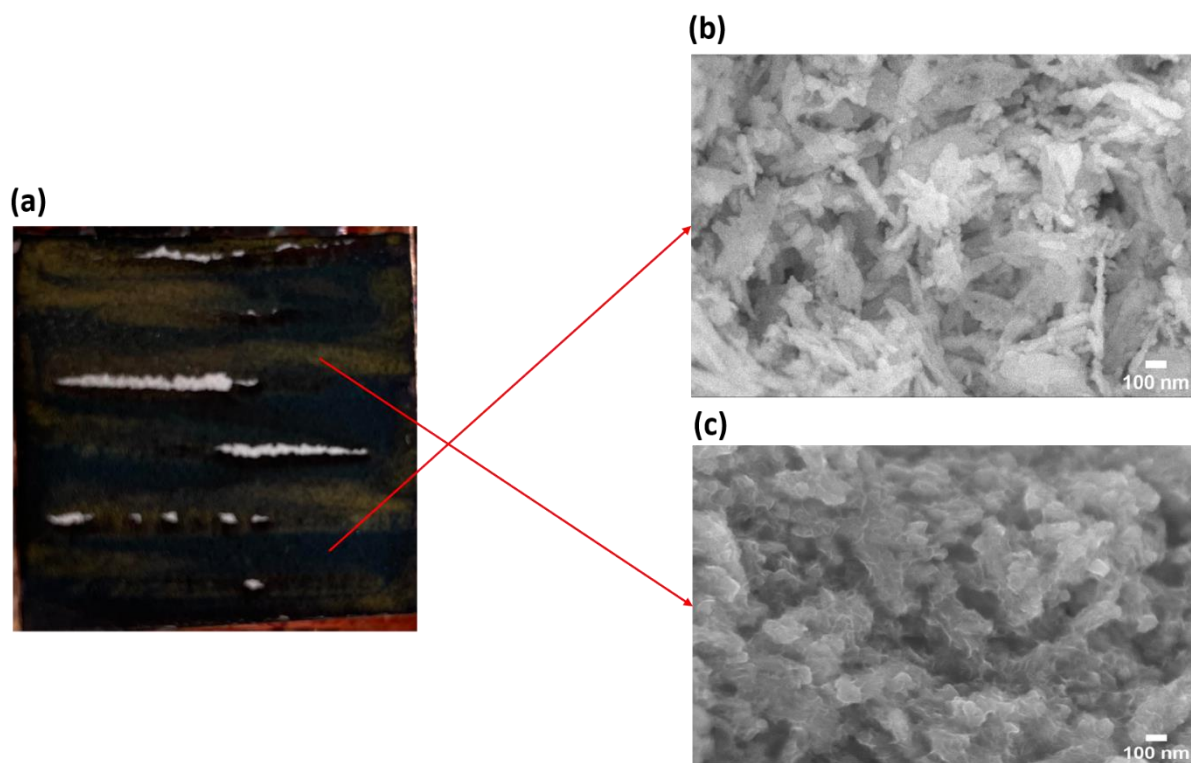


**Fig. S13.** Investigation of discolored areas (yellow spots) that were visible on electrodes after the electrochemical reaction. (a) Photograph of the electrode after testing with the Serpentine flow compartment (b) 50k magnification SEM image of an electrode area after electrochemical testing without visible discoloration. The particle morphology resembles the electrode measured with the Shifted flow compartment shown earlier. (c) 50k magnification SEM image of an electrode area after electrochemical testing showing a visible yellow discoloration. Here, the particle morphology changed considerably and shows a “nano-flower” type structure.

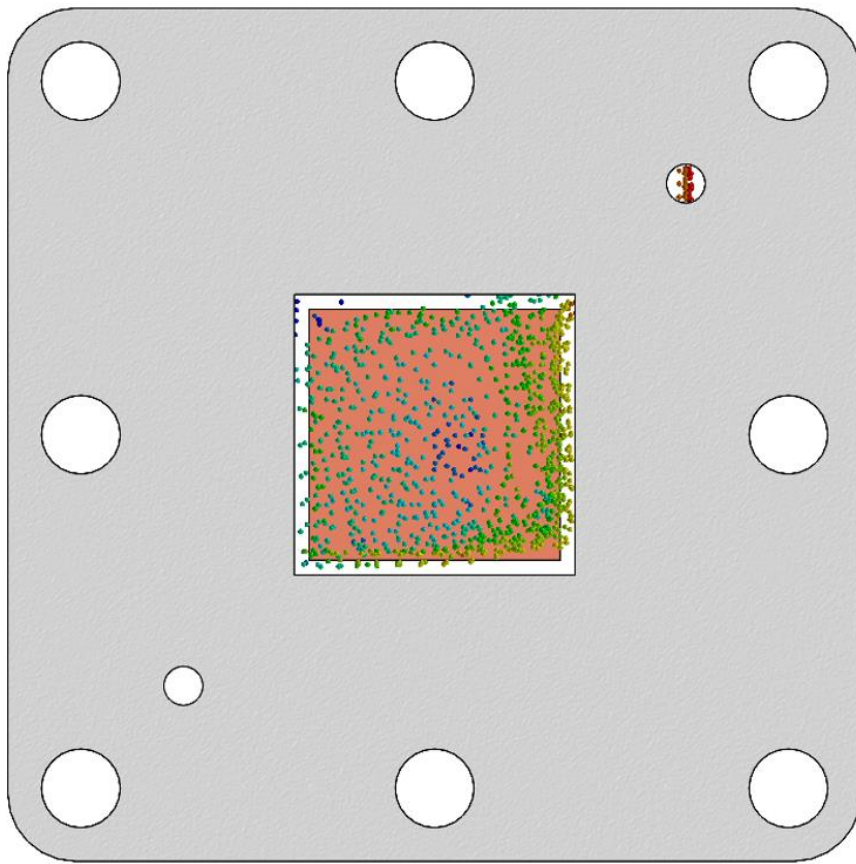


**Fig. S14.** An exemplary model used for the particle study. The copper electrode surface is shown in the typical reddish copper colour. The copper surface is designated as the origin of the emerging gas bubbles.

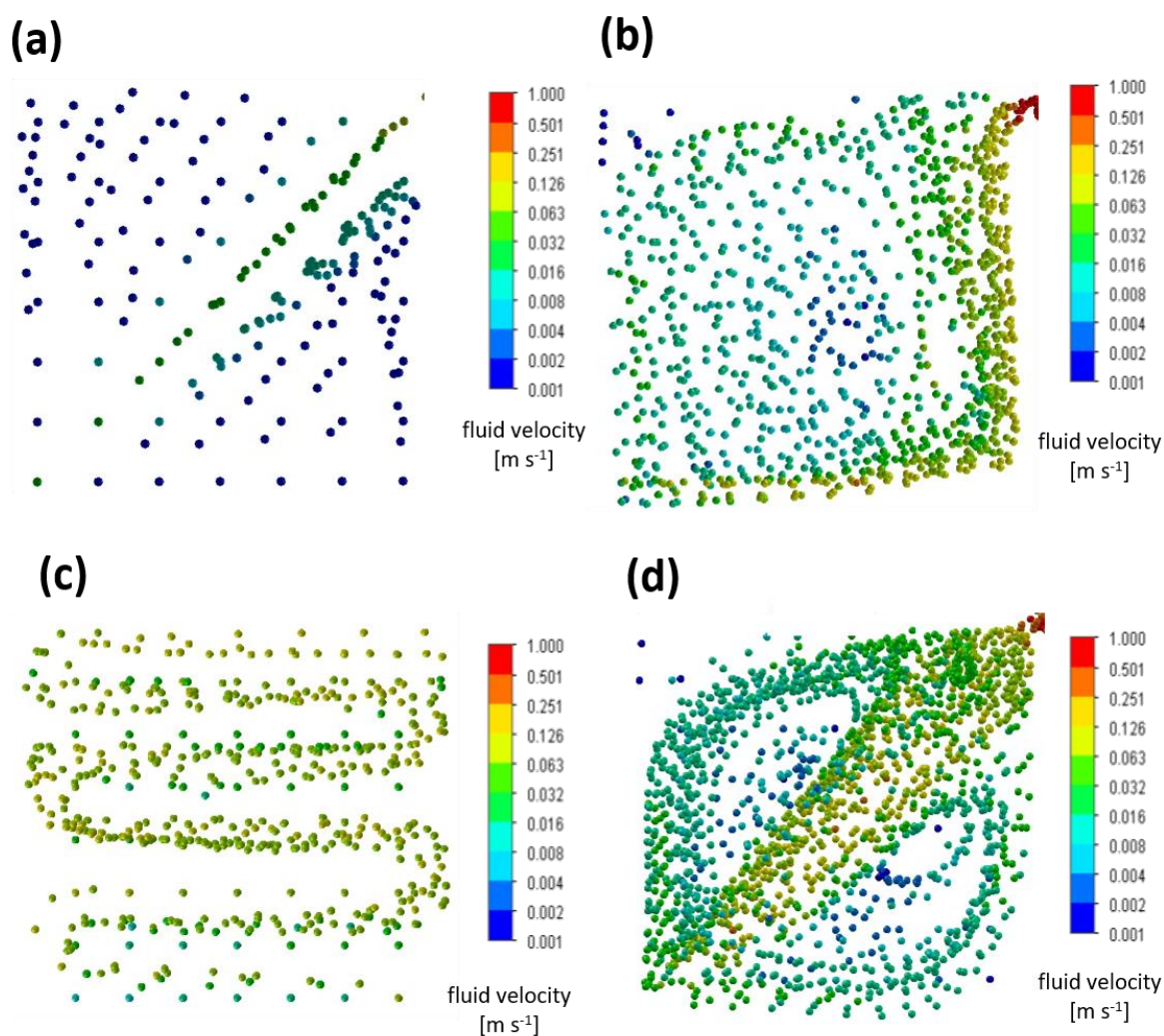


**Fig. S15.** Gas bubble formation on the here studied copper GDEs for various flow compartment geometries. CFD simulations coupled with a particle study comprising nitrogen particles that arise from the cathode surface with a volume flow rate of  $1 \text{ ml min}^{-1}$ . Gas bubbles were enlarged to 5 times their simulated size ( $100 \text{ }\mu\text{m}$ ) for better visual comparison. Coupled CFD simulation with particle study on (a) Linear wide flow compartment, (b) Shifted flow compartment, (c) Serpentine flow compartment and (d) Linear flow compartment. Additional information: A higher visual density of gas bubbles indicates a very good transport away from the cathode surface, whereas a low density of bubbles and slow velocity indicate areas with non-ideal bubble transport.

## **Supplementary discussion II**

This section further elaborates on the gas phase products observed in the catholyte (crossover experiments). We propose that not all products are produced in the exact same geometric location due to mass transport gradients in the catalyst layer. In our previous publication, the product selectivity zone model was proposed, explaining our observations in the crossover experiments.<sup>1</sup> Based on the selectivity zone model, the first zone (closest to the gas supply) is the C<sub>2+</sub> zone, where the most significant amount of C<sub>2+</sub> products (ethylene, ethanol and propanol) are produced. The C<sub>2+</sub> zone is followed by the C<sub>1</sub> zone and, finally, the H<sub>2</sub> zone, which is most far away from the gas supply. Once the current density increases, CO<sub>2</sub> depletes inside the catalyst layer, and the hydrogen zone will grow if mass transport becomes limiting. Instead of a three-zone selectivity model, we propose a two-zone selectivity model, which better fits our observed experimental results in the studied system. In Fig. S16a, we show a prototypical selectivity zone model for the low current density regime and in Fig. S16b for the high current density regime. The difference between low and high current density regimes is the relative ratio of the hydrogen zone "H<sub>2</sub> zone" compared to the "CO<sub>2</sub>RR zone". In the low current density regime shown in Fig. S16a, the hydrogen zone is small compared to the high current density case, and the depletion of CO<sub>2</sub> inside the layer is less pronounced. In the low current density regime, only minimal amounts of hydrogen were detected in the catholyte and almost no CO<sub>2</sub>RR products. In the high current density regime, more CO<sub>2</sub> gets consumed, which results in a steeper decline of CO<sub>2</sub> concentration inside the catalyst layer. This, in turn, creates a larger portion of the catalyst layer, which will produce hydrogen, as indicated in Fig. S16b by a larger H<sub>2</sub> zone. In the high current density regime, we also experimentally observed an increasing ethylene crossover which was much less pronounced than the effect on hydrogen. According to the model, ethylene will be produced at higher rates in regions where CO<sub>2</sub> supply can be maintained and, at the same time, in regions with higher alkalinity. We acknowledge that the reality is more complex than the selectivity zone model suggests, and the model cannot account for every experimental observation as no CO or CH<sub>4</sub> crossover was detected.

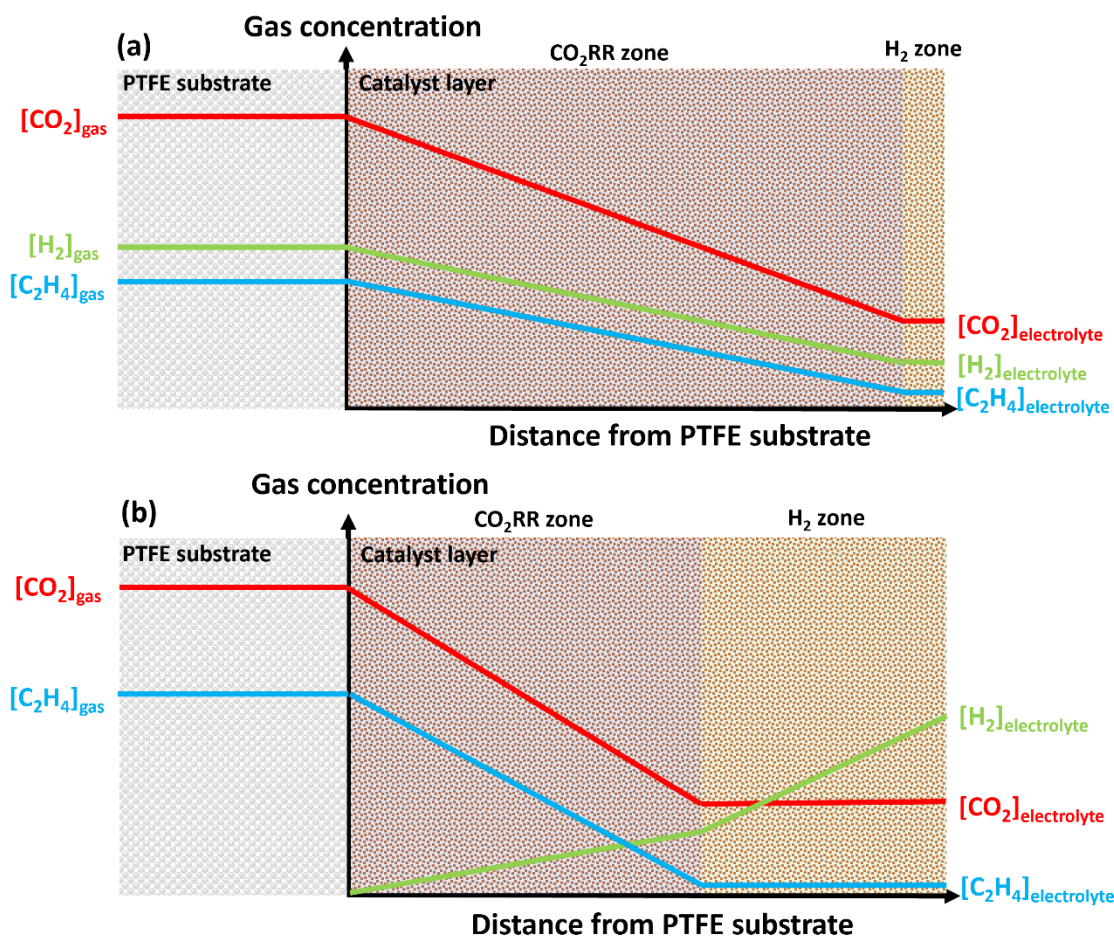


**Fig. S16.** Modified two-zone selectivity model shown for (a) low current density regime and (b) high current density regime.

## Supplemental Videos

SI Video 1. Particle study performed on the Linear wide compartment.

SI Video 2. Particle study performed on the Shifted compartment.

SI Video 3. Particle study performed on the Serpentine compartment.

SI Video 4. Particle study performed on the Linear compartment.

## References

1. T. Möller, T. Ngo Thanh, X. Wang, W. Ju, Z. Jovanov and P. Strasser, *Energy & Environmental Science*, 2021, **14**, 5995-6006.